Available online at www.sciencedirect.com
ScienceDirect
Geochimica et Cosmochimica Acta 74 (2010) 3721–3734
Geochimica et Cosmochimica Acta
www.elsevier.com/locate/gca

Biomineralization of lepidocrocite and goethite by nitrate-reducing Fe(II)-oxidizing bacteria: Effect of pH, bicarbonate, phosphate, and humic acids

Philip Larese-Casanova *, Stefan B. Haderlein, Andreas Kappler

Center for Applied Geosciences, Eberhard-Karls-University Tuebingen, Sigwartstrasse 10, 72076 Tübingen, Germany

Received 21 October 2009; accepted in revised form 31 March 2010; available online 7 April 2010

Abstract

Fe(III) solid phases are the products of Fe(II) oxidation by Fe(II)-oxidizing bacteria, but the Fe(III) phases reported to form within growth experiments are, at times, poorly crystalline and therefore difficult to identify, possibly due to the presence of ligands (e.g., phosphate, carbonate) that complex iron and disrupt iron (hydr)oxide precipitation. The scope of this study was to investigate the influences of geochemical solution conditions (pH, carbonate, phosphate, humic acids) on the Fe(II) oxidation rate and Fe(III) mineralogy. Fe(III) mineral characterization was performed using ^{57}Fe-Mössbauer spectroscopy and μ-X-ray diffraction after oxidation of dissolved Fe(II) within Mops-buffered cell suspensions of *Acidovorax* sp. BoFeN1, a nitrate-reducing, Fe(II)-oxidizing bacterium. Lepidocrocite (γ-FeOOH) (90%), which also forms after chemical oxidation of Fe(II) by dissolved O_2, and goethite (α-FeOOH) (10%) were produced at pH 7.0 in the absence of any strongly complexing ligands. Higher solution pH, increasing concentrations of carbonate species, and increasing concentrations of humic acids promoted goethite formation and caused little or no changes in Fe(II) oxidation rates. Phosphate species resulted in Fe(III) solids unidentifiable to our methods and significantly slowed Fe(II) oxidation rates. Our results suggest that Fe(III) mineralogy formed by bacterial Fe(II) oxidation is strongly influenced by solution chemistry, and the geochemical conditions studied here suggest lepidocrocite and goethite may coexist in aquatic environments where nitrate-reducing, Fe(II)-oxidizing bacteria are active.

1. INTRODUCTION

Aerobic and anaerobic iron(II)-oxidizing bacteria contribute to iron, carbon, and nutrient cycling within a variety of freshwater, groundwater, and marine environments (Straub and Buchholz-Cleven, 1998; Emerson and Moyer, 2002; Emerson and Weiss, 2004; Straub et al., 2004). Although having diverse phylogenies, these bacteria have a common physiological process of deriving energy from the oxidation of Fe(II), usually soluble, to Fe(III), which is poorly soluble in waters of circumneutral pH and can precipitate as various iron (hydr)oxides. Iron (hydr)oxides are important environmental materials for microbial Fe(III) respiration (Lovley, 1991), solute sorption and coprecipitation (Charlet and Manceau, 1992), and pollutant redox transformations (Klausen et al., 1995). Their electronic, surficial, and size-dependant properties can differ widely among the types of oxides and among the processes of formation (e.g., abiogenic vs. biogenic). Therefore, understanding the identity, size, and morphology of biogenic iron oxides formed from Fe(II)-oxidizing bacteria can be helpful to understand not only cell metabolism but also the reactive nature of environmental iron oxides.

* Corresponding author. Present address: Department of Geology & Geophysics, Yale University, P.O. Box 208109, New Haven, CT 06520-8109, USA. Tel.: +1 203 436 4049; fax: +1 203 432 3134.
E-mail address: philip.larese-casanova@yale.edu (P. Larese-Casanova).

0016-7037/$ - see front matter © 2010 Elsevier Ltd. All rights reserved.
doi:10.1016/j.gca.2010.03.037

Fe(II) oxidation by different bacteria have produced Fe(III) minerals of different identities and morphologies—likely by means of a combination of abiotic or biotically influenced Fe(III) precipitation processes—that include poorly crystalline (hydr)oxides (Emerson and Revsbech, 1994; Croal et al., 2004), ferrihydrite (Banfield et al., 2000; Lack et al., 2002; Kennedy et al., 2003), goethite (Banfield et al., 2000; Kennedy et al., 2003; Kappler and Newman, 2004; Kappler et al., 2005; Senko et al., 2005a,b; Miot et al., 2009c; Hohmann et al., 2010), lepidocrocite (Kappler and Newman, 2004), magnetite (Chaudhuri et al., 2001), green rust (Chaudhuri et al., 2001), and Fe(III)-phosphates (Miot et al., 2009a,b). The observed Fe(III) mineral diversity may be a result of different mechanisms of enzymatic Fe(II) oxidation, different cell–Fe(III) interactions, and different geochemical solution conditions. Specific factors studied so far include Fe(III) nucleation and templating by cell membranes and exopolymers (Chan et al., 2004; Hallberg and Ferris, 2004; Miot et al., 2009b), rate of Fe(II) oxidation (Senko et al., 2005a), formation of locally acidic environments (Kappler and Newman, 2004; Hegler et al., 2008), and Fe(III) precipitation locations either within, on, or away from cell membranes (Miot et al., 2009b; Schaedler et al., 2009).

However, there is a lack of information on the influences of geochemical solution conditions on the Fe(III) mineralogy formed from anaerobic Fe(II)-oxidizing bacteria. It is reasonable to expect geochemical conditions will strongly influence Fe(III) mineralogy because solution pH and dissolved ions govern iron solubility, speciation, and redox potential. For example, dissolved carbonate and phosphate (two anions usually present within growth medium) can form soluble complexes and precipitates with both Fe(II) and Fe(III), and there is some evidence that solid-phase Fe(II)-carbonates (e.g., siderite, $FeCO_3$) and Fe(II)-phosphates (e.g., vivianite $Fe_3(PO_4)_2$) can limit the bioavailability of aqueous Fe(II) for oxidation (Kappler and Newman, 2004). Inorganic oxyanions can also coprecipitate with Fe(III) (hydr)oxides and disrupt crystallinity (Thibault et al., 2009) and can even direct the formation of particular phases (e.g., goethite in preference to lepidocrocite in the presence of carbonate) (Schwertmann and Cornell, 2000; Châtellier et al., 2004). Consequently, some studies report a poorly crystalline Fe(III) phase after microbial Fe(II) oxidation within medium rich in phosphate (Croal et al., 2004; Miot et al., 2009a,b; Posth et al., 2010), and others report goethite formation in low- or no-phosphate, carbonate-rich solutions (Senko et al., 2005a,b; Hohmann et al., 2010; Posth et al., 2010). Finally, even the same microorganism, e.g., the nitrate-reducing, Fe(II)-oxidizing strain *Acidovorax* sp. strain BoFeN1, has produced different minerals (Fe(III)-phosphate, ferrihydrite, goethite or lepidocrocite) within cultures of different medium composition (Kappler et al., 2005; Miot et al., 2009a,b; Hohmann et al., 2010).

Because cell culture growth medium usually contains strongly iron-complexing ions, the Fe(III) minerals formed from bacterial Fe(II) oxidation within growth cultures are likely different than the Fe(III) minerals that can form by bacterial oxidation of aqueous Fe(II) alone, and may not well represent naturally occurring Fe(III) minerals. This work characterizes Fe(III) mineralogy formed by anaerobic Fe(II)-oxidizing bacteria within simplified solution conditions that more closely approximate natural settings. For one, only aqueous Fe(II) was provided and not solid Fe(II) which may sequester Fe(II) from bacteria or influence Fe(III) mineral formation pathways. Second, resting cell suspensions were used after harvesting from growth cultures in order to avoid the complexing anions, nutrients, vitamins, etc. from growth medium. This approach established a baseline condition for determining the primary Fe(III) mineralogy and allowed for testing individual geochemical solution parameters that are pertinent to anoxic groundwater environments and laboratory batch studies.

An anaerobic, neutrophilic, nitrate-reducing, Fe(II)-oxidizing bacterium was chosen because its metabolic requirements allow studying iron precipitation processes at geochemically well-defined conditions. *Acidovorax* sp. BoFeN1 is a β-proteobacterium, was first isolated from a freshwater lake sediment, uses nitrate as a terminal electron acceptor and acetate as a co-substrate during Fe(II) oxidation, and does not require O_2 or light (Kappler et al., 2005; Muehe et al., 2009). Grown BoFeN1 cells were suspended in Good's buffered solutions (Good and Izawa, 1972) containing dissolved Fe(II), nitrate, acetate, and sodium chloride, and were subjected to different solution pH values and additions of carbonate, phosphate, and dissolved humic substances. Fe(II) oxidation was characterized with ^{57}Fe-Mössbauer spectroscopy and powder micro-X-ray diffraction (μ-XRD).

2. METHODS

2.1. Reagents

All chemical reagents for growth medium and Fe(II) oxidation experiments were purchased at high purity (typically ACS reagent or certified grade). Anoxic growth medium was a modified version of freshwater medium from Ehrenreich and Widdel (1994) and was prepared according to Hegler et al. (2008). Anoxic stock solutions of Mops (3-(*N*-morpholino)propanesulfonic acid), Mes (2-(*N*-morpholino)ethanesulfonic acid), NaCl, $NaHCO_3$, Na_2HPO_4, NaOH, and $NaCH_3COO$ were prepared using N_2-purged, deoxygenated, deionized water within an anoxic glove box with a 100% N_2 atmosphere. HCl solution was made by diluting N_2-purged concentrated HCl with deoxygenated, deionized water. An acidic solution of ^{57}Fe(II) (99% pure, Chemgas) was made by dissolving ^{57}Fe(0) powder (96 atom %) in anoxic 1 M HCl solution and filtered (PTFE, 0.45 μm) prior to use.

A solution of Pahokee Peat Humic Acid ("PPHA", purchased from the International Humic Substance Society (IHSS)) was prepared by adding the dried humics to deoxygenated, deionized water containing about 2 mM of NaOH to facilitate dissolution. After 2 h, the solution was filtered (PTFE, 0.45 μm), and the dissolved organic carbon (DOC) content was determined using a total organic carbon analyzer. This solution was used on the same day as preparation to avoid changes that can occur during storage.

2.2. *Acidovorax* sp. BoFeN1 cultivation

BoFeN1 cells were first grown within anoxic medium containing acetate as the carbon substrate, Fe(II) as an electron source, and nitrate as the terminal electron acceptor as described in Kappler et al. (2005) until maximum growth represented by late stationary growth phase. In order to minimize the amount of iron particles (which could act as nucleation sites) transferred to later cell cultures, an inoculum of cells was then transferred to anoxic medium for growth with acetate and nitrate (without Fe(II)) according to the following procedure. Sixty milliliters of anoxic medium was first distributed to sterile 120-ml serum bottles and flushed with 80/20 N_2/CO_2 gas. Sterile, anoxic solutions of nitrate and acetate were added to final concentrations of 5 and 10 mM, respectively. An inoculum of BoFeN1 cells was added to a final concentration of 1% (v/v). Cultures were incubated at 30 °C until late stationary growth phase. A second transfer of cells was performed in the same manner. After maximum growth until late stationary phase, these cells were collected by combining the contents of several cultures, centrifuging for 12 min at 5000*g*, and washing twice with a deoxygenated solution of 30 mM Mops buffer (pH 7.0) and 30 mM NaCl. Cells were resuspended within the Mops–NaCl solution for a final stock solution, and its cell density was determined by cell counting with a light microscope and a Thoma® grid slide.

2.3. Fe(II) oxidation experiments

Cell suspensions were prepared within the anoxic chamber. ^{57}Fe(II) was first added to a concentration of approximately 3 mM within deoxygenated, deionized water containing 30 mM NaCl, 30 mM Mops buffer, 3 mM nitrate, and 0.3 mM acetate. A small amount of acetate was necessary to produce ATP for reverse electron transport during Fe(II) oxidation; without acetate, Fe(II) oxidation by BoFeN1 is insignificant (Muehe et al., 2009). Solution pH was adjusted to 7.0, unless otherwise noted, by addition of 0.5 M NaOH or HCl. Mes buffer was used instead of Mops for one suspension conducted at pH 6.3. The Mops and Mes buffers were chosen because they demonstrate no significant complexation with dissolved metal cations (Yu et al., 1997). The Fe(II) solution was allowed to equilibrate for at least 2 h before filtration through 0.45 μm nylon filters to remove any unseen iron precipitates formed from the addition of Fe(II). For certain experiments, a bicarbonate solution or phosphate solution was added to concentrations of 0.2, 1.0, or 3.0 mM followed by re-adjustment of solution pH to 7.0. In other experiments, PPHA was added to final dissolved organic carbon (DOC) concentrations of 0.2, 1.0, or 3.0 mM, and solutions were progressively darker with greater DOC concentrations. The reported DOC concentrations within cell suspension experiments are calculated DOC concentrations based on the known volume of PPHA stock solution added. No attempts were made to directly measure DOC after PPHA addition because we assumed the Mops buffer and any cellular exudates would interfere with the measurement. In all experiments, predetermined volumes of BoFeN1 cell stock suspension were added, providing a translucent white color to the suspension. One BoFeN1 cell stock solution was used for all cell suspensions within each set (varying pH, total carbonate, total phosphate, or DOC), and we assume cells behaved identically among suspensions within each set. The serum bottles were crimp-sealed with butyl rubber stoppers, incubated at 26 °C in the dark, and shaken by hand periodically.

Samples for aqueous Fe(II) measurements were removed with a nitrogen-flushed syringe and needle and filtered (PTFE, 0.45 μm) through syringe-tip filters. Samples were taken immediately after crimp-sealing ($Fe(II)_{initial}$), during the course of the experiments, and at the determined endpoint ($Fe(II)_{final}$), which was between 36 and 190 h.

2.4. Chemical analyses

Aqueous Fe(II) concentrations were determined with the ferrozine method (Stookey, 1970). Dissolved phosphate concentrations were measured using a modified molybdenum blue method according to Laskov et al. (2007).

Concentrations of dissolved nitrate and nitrite were estimated using colorimetric strips (Merck) that were dipped into filtered samples and whose color intensity was compared to a given calibration scale. While we acknowledge this method is semi-quantitative, it was not possible to directly measure nitrate and nitrite concentrations using our ion chromatography due to the interference of the background concentrations of Mops buffer, chloride electrolyte, and Fe(II). For the same reasons, it was not possible to measure acetate concentrations.

2.5. Mineral analyses

Within the anoxic glove box, solids from suspensions were filtered onto 13 mm diameter, 0.45 μm, removable syringe-tip filter membranes (mixed cellulose esters, 0.45 μm) and preserved between two layers of oxygen-impermeable Kapton® tape for ^{57}Fe-Mössbauer analysis. The analysis was performed with a ^{57}Co source at room temperature with linear acceleration in transmission mode. The temperature of the sample was varied with a Janis cryostat with a helium atmosphere. Spectra were calibrated against spectra of α-Fe(0) foil. For spectra interpretation, Recoil® software and Voigt-based models were used.

The solids used for Mössbauer analysis were retained within the Kapton® tape and stored within the anoxic glove box (up to 3 weeks) for later analysis by X-ray diffraction with a Bruker D8 Discover μ-X-ray diffractometer with Co Kα radiation focused to a 300-μm diameter spot size. The sample for scanning electron microscopy was placed on an aluminum grid, sputter-coated with platinum, and imaged with a LEO 1450 VP microscope. No attempt was made to wash the solids or preserve whole cells for imaging.

3. RESULTS AND DISCUSSION

3.1. Fe(II) oxidation and nitrate reduction by *Acidovorax* sp. strain BoFeN1 in cell suspensions

Sustained growth of *Acidovorax* sp. BoFeN1 is possible with Fe(II) and acetate as substrates and nitrate as a

terminal electron acceptor within anoxic freshwater medium (Kappler et al., 2005; Miot et al., 2009a,b; Muehe et al., 2009; Schaedler et al., 2009; Hohmann et al., 2010). Here, we demonstrated that BoFeN1 cells can also oxidize aqueous Fe(II) within resting cell suspensions (Fig. 1 and Table 1). Aqueous Fe(II) disappeared from solution over the course of 36 h within a Mops buffer suspension containing approximately 3.6×10^8 cells ml^{-1} of BoFeN1, 3.0 mM nitrate, and 0.3 mM acetate. Oxidation of Fe(II) to Fe(III) was visually observed as the suspension color changed from whitish translucent (due to the high density of cells) to yellow to orange, and the formed precipitates eventually settled, leaving a transparent supernatant. Nitrite was formed concurrently with Fe(II) oxidation and accounted for 55% of the electrons donated from the initial 3300 μM Fe(II) oxidized. The remaining electrons from oxidized Fe(II) may have formed more nitrite not resolved by the colorimetric strips or other nitrate reduction products such as $N_{2(g)}$, $N_2O_{(g)}$, or NH_4^+, which were not investigated. Nitrite may have chemically oxidized some aqueous Fe(II), Fe(II) associated with cell surfaces (Coby and Picardal, 2005; Kappler et al., in press), or Fe(II) sorbing on Fe(III) mineral surfaces (Sørensen and Thorling, 1991), although these processes are important only under higher nitrite and oxide concentrations and are likely to be kinetically slower than microbially catalyzed Fe(II) oxidation (Kappler et al., 2005). The simultaneous Fe(II) oxidation and nitrite formation was evident only after a brief lag period likely due to the preferential oxidation of acetate which was already observed in growing cultures of BoFeN1 (Kappler et al., 2005). No Fe(II) loss, Fe(III) mineral formation, or nitrite formation was observed in an uninoculated control.

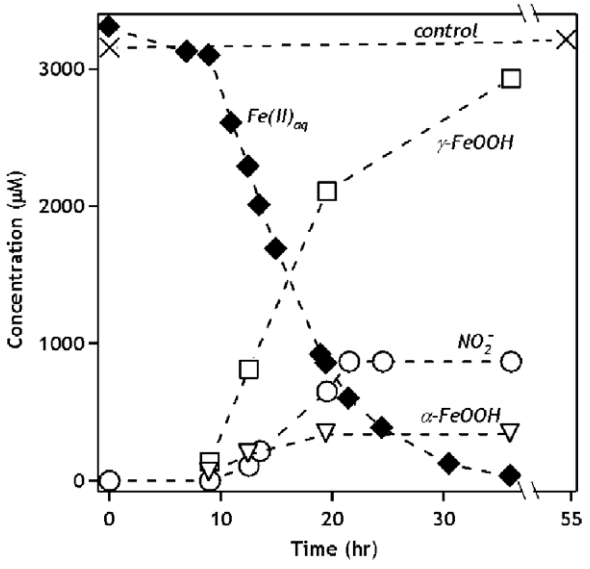

Fig. 1. Aqueous Fe(II) loss (closed diamonds), nitrite formation (open circles), lepidocrocite formation (open squares), and goethite formation (open triangles) over time within a cell suspension of *Acidovorax* sp. BoFeN1 at an initial pH of 7.0. The X markers are aqueous Fe(II) concentrations within an uninoculated control batch reactor. Additional information for solution conditions and some sample points is listed in Table 1. The marker for the Fe(II) species within the Mössbauer spectrum measured at 9.5 h was omitted for clarity.

3.2. Fe(III) mineral formation during Fe(II) oxidation by *Acidovorax* sp. strain BoFeN1

Aliquots of the cell suspension were filtered at selected time points, and filtered minerals were analyzed with Mössbauer spectroscopy in order to demonstrate oxidation of Fe(II) to Fe(III) and to identify the formed minerals. The two iron oxidation states are most readily distinguished by the different values of average center shift (⟨CS⟩) (0.3–0.6 for high-spin octahedral Fe(III) and 1.0–1.4 for high-spin octahedral Fe(II)). This modeled center shift in concert with modeled values of average quadrupole splitting (⟨QS⟩), average hyperfine field (⟨H⟩), and most probable hyperfine field (H_p), can be compared to pure iron mineral standards for mineral identification.

Within the first few minutes of aqueous Fe(II) exposure to BoFeN1 cells, and prior to any significant aqueous Fe(II) loss or suspension color change, both Fe(II) and Fe(III) were found associated with filtered BoFeN1 cells (Fig. 2) as an Fe(II) doublet (⟨CS⟩ 1.32 mm s^{-1}, ⟨QS⟩ 2.92 mm s^{-1}) and an Fe(III) doublet (0.48 mm s^{-1}, 0.76 mm s^{-1}) (see 0 h spectrum in Fig. 2). These values, and the lack of any hyperfine magnetic order at this analysis temperature (77 K), best resemble those for sorbed Fe(II) and Fe(III) cations on cell membranes (Rancourt et al., 2005) or the mixed-valent iron hydroxide green rust (Génin et al., 1998).

By 9 h, only a minor amount of solid-phase Fe(II) was detected, and all Fe(III) was evident either as lepidocrocite or goethite (Fig. 2 and Table 2). The lepidocrocite sextet phase was apparent based on its lower hyperfine field value (about 45 T) and symmetrical arrangement of its six peak positions caused by its low quadrupole splitting value (0.02 mm s^{-1}). In contrast, goethite was clearly identified by its unique quadrupole splitting of −0.20 mm s^{-1} (close to the standard value of −0.25 mm s^{-1}) and larger hyperfine field value (about 50 T).

More rapid bacterial Fe(II) oxidation proceeded beyond 9 h and resulted in additional formation of lepidocrocite and goethite, and the abundances of these two phases were monitored over time in order to observe the rate and extent of the formation of each phase. The areas of each modeled phase were used to estimate the physical abundance at the sample time according to the following equations:

$$\mu\text{moles lepidocrocite} = (\text{fraction spectral area lepidocrocite}) \times (\text{total } \mu\text{moles Fe(II)}_{aq} \text{ removed})$$

$$\mu\text{moles goethite} = (\text{fraction spectral area goethite}) \times (\text{total } \mu\text{moles Fe(II)}_{aq} \text{ removed})$$

with the assumption that the recoilless fractions of the two phases are identical. After the formation of roughly similar abundances of lepidocrocite and goethite at 9 h, lepidocrocite grew more rapidly and to a far greater extent compared to goethite, whose concentration leveled off by 20 h. After 36 h, the primary Fe(III) mineral formed was lepidocrocite,

Table 1
Solution conditions and Fe(III) mineral formation for cell suspensions of *Acidovorax* sp. BoFeN1 with aqueous Fe(II).[a]

Sample No.	Additive (mM)	Time (h)	$pH_{initial}$	pH_{final}	Cell density cells (ml^{-1})	$Fe(II)_{initial}$ (μM)	$Fe(II)_{final}$ (μM)	$Fe(II)_{reacted}$ (μmoles)	Lepidocrocite (μmoles)	Goethite (μmoles)
Vary reaction time[b]										
1	—	0	7.05	nm[c]	3.6×10^8	3302	nm	nm	nd[d,e]	nd
2	—	9	7.05	nm	3.6×10^8	3302	3095	15.5	10.7	4.4
3	—	12.5	7.05	nm	3.6×10^8	3302	2285	76.3	61.1	14.4
4	—	19.5	7.05	nm	3.6×10^8	3302	854	183.6	158.3	25.3
5	—	36	7.05	6.78	3.6×10^8	3302	30	245.4	219.9	25.5
Vary solution pH										
6	—	154	6.30	6.19	6.7×10^7	2841	1310	30.6	30.6	0.0
7	—	154	7.02	6.70	6.7×10^7	2960	11	59.0	54.9	4.1
8	—	106	7.75	7.31	6.7×10^7	2946	0	58.9	24.9	34.0
Vary HCO_3^- concentration										
9	—	49.8	7.01	6.84	4.5×10^7	2807	584	44.5	41.6	2.8
10	0.2	49.8	7.04	6.84	4.5×10^7	2857	200	53.1	49.0	4.1
11	1.0	49.8	6.97	6.80	4.5×10^7	2840	223	52.3	47.1	5.3
12	3.0	49.8	6.94	6.76	4.5×10^7	2837	242	51.9	42.9	9.0
Vary HPO_4^{2-} concentration										
13	—	68.3	6.96	6.70	5.3×10^7	2888	1018	37.4	33.8	3.6
14	0.2	141.3	6.97	6.70	5.3×10^7	2888	59	56.9	nd	nd
15	1.0	165	6.97	6.80	5.3×10^7	2970	670	46.0	nd	nd
16	3.0	189	6.97	6.92	5.3×10^7	2900	2305	11.9	nd	nd
Vary PPHA concentration										
17	—	154	7.02	6.70	6.7×10^7	2960	11	59.0	54.9	4.1
18	0.2	154	7.02	6.71	6.7×10^7	2934	29	58.1	50.6	7.5
19	1.0	154	7.02	6.71	6.7×10^7	2935	35	58.0	26.2	31.8
20	3.0	106	7.02	6.70	6.7×10^7	2925	273	53.0	nd	nd

[a] All cell suspensions contained 3.0 mM $NaNO_3$, 0.3 mM $NaCH_3COO$, 30 mM NaCl, and 30 mM of a Good's buffer, which was Mops for all suspensions except for 6.3 (Mes).
[b] Sample numbers 1–5 were taken from one cell suspension of 75 ml initial volume.
[c] Not measured.
[d] Not detected.
[e] Sample 1 was found to have an Fe(II) and an Fe(III) species within its Mössbauer spectrum but no lepidocrocite or goethite (Fig. 2).

consistent with the strong orange color of the suspension. Lepidocrocite was confirmed within a μ-XRD pattern, which shows many well-resolved reflections indicative of a well-crystalline nature (Fig. 3a). Goethite reflections were not clearly observed within the pattern, possibly because the crystallites were too small or covered by lepidocrocite. An SEM image of the solids confirms the crystalline nature of some of the solids (Fig. 3b), which assume a tabular morphology of wide particle size distribution (50–1000 nm). Distinction between lepidocrocite and goethite was not possible at this spatial resolution.

3.3. Factors controlling lepidocrocite and goethite formation during microbial and chemical Fe(II) oxidation

Formation of a Fe(III) (hydr)oxide (such as ferrihydrite, lepidocrocite, or goethite) as opposed to a Fe(III) oxide (such as hematite or maghemite) after bacterial oxidation of dissolved Fe(II) is expected because the Fe(III) (hydr)oxides readily form after abiotic oxidation of Fe(II) and hydrolysis of Fe(III) near room temperature. Specific Fe(III) hydroxides can be synthesized chemically by controlling the type of oxidant (O_2 or H_2O_2), the rate of Fe(II) oxidation, solution pH, Fe(II) concentration, or presence of foreign ions such as bicarbonate, among other solution properties (Schwertmann and Cornell, 2000; Cornell and Schwertmann, 2003). Here, the formation of primarily lepidocrocite within anoxic BoFeN1 cell suspensions at pH 7 is consistent with the formation of lepidocrocite within anoxic Fe(II) solutions at pH 7 bubbled with O_2 (Schwertmann and Cornell, 2000; Châtellier et al., 2001) in the absence of any iron-complexing anions or bacteria cells. In fact, we confirmed pure lepidocrocite forms by aqueous Fe(II) oxidation with O_2 within our specific batch reactor solution containing $^{57}Fe(II)$, NO_3^-, acetate, NaCl, and Mops buffer at an initial pH of 7.26 (experiment details and results are provided within Electronic Annex). There is virtually no difference between the primary Fe(III) phase formed from bacterial Fe(II) oxidation and the sole Fe(III) phase formed abiotically with O_2, indicating that the mode of Fe(II) oxidation (biotic or abiotic) does not determine Fe(III) mineralogy and that the Fe(III) precipitation process was controlled by the geochemical condition of the solution alone.

A small amount (10% of Fe(III)) of goethite did form, nevertheless, and it is unknown whether this phase resulted from purely geochemical precipitation reactions or from cellular material influences. Because no goethite was found

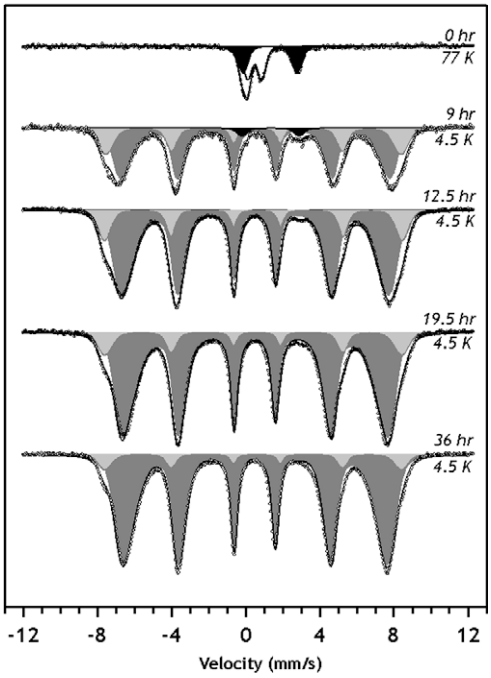

Fig. 2. Mössbauer spectra of solids taken at selected time points from the batch reactor in Fig. 1. Dark grey sextets are lepidocrocite, light grey sextets are goethite, black shaded doublets are Fe(II) species, and the white doublet is an Fe(III) specie. The temperature of analysis is indicated below each spectrum. Model parameters for each spectrum are listed in Table 2.

by abiotic Fe(II) oxidation with O_2, its presence is likely due to some physical or metabolic feature of the cells. Goethite can form by abiotic Fe(II) oxidation at circumneutral pH in the presence of high concentrations of bicarbonate (Schwertmann and Cornell, 2000; Cornell and Schwertmann, 2003), and here it is likely that some dissolved carbonate species formed from acetate oxidation. Carbonate species are thought to direct iron oxidation towards goethite precipitation instead of lepidocrocite by promoting the corner-linked rows of Fe(III) octahedra sheets in goethite in favor of the edge-linked rows in lepidocrocite during Fe(III) (hydr)oxide nucleation and crystal growth (Carlson and Schwertmann, 1990). In a similar manner, membrane surface and periplasm functional groups may have complexed Fe(III) and promoted goethite formation. Carboxyl functional groups on cellular material have been implicated with Fe(III) (hydr)oxide formation (Chan et al., 2009). Any influence by either dissolved carbonate species or membrane functional groups may have been temporary, as both may have been exhausted during early goethite formation, which stopped prior to full Fe(II) oxidation.

This report is the first of any nitrate-reducing, Fe(II)-oxidizing bacteria producing crystalline lepidocrocite, although there are reports of some lepidocrocite formation by phototrophic Fe(II)-oxidizing bacteria under growth conditions (Kappler and Newman, 2004) and lepidocrocite occurrence with other iron minerals associated with aerobic microbial Fe(II) oxidation in nature (Chan et al., 2004). We suspect the main reason we see primarily lepidocrocite during strictly biotic, non-growth Fe(II) oxidation is because we used a cell suspension without iron-complexing anions such as carbonate or phosphate. Other cell suspension experiments at circumneutral pH report Fe(III) mineral formation, but these used a carbonate buffer, and goethite (Senko et al., 2005a,b), or in one case ferrihydrite (Lack et al., 2002), was the primary Fe(III) phase formed. In the case of Kappler and Newman (2004), the lepidocrocite was noticeable only at the end of the experiment, possibly after the influence of bicarbonate was exhausted.

Because lepidocrocite and goethite formation are reported to be sensitive to dissolved carbonate species, the influence of dissolved carbonate, as well as solution pH, phosphate, and humic acids, on the abundances of lepidocrocite and goethite was tested within the following sections.

3.4. Influence of solution pH

Three pH values (6.3, 7.0, and 7.7) were tested to examine the influence of solution pH on the oxidation rate of aqueous Fe(II) and the mineralogy of Fe(III). For higher pH values, the rate of Fe(II) oxidation increased, and the duration of the lag phase decreased (Fig. 4a). The extended lag period at pH 6.3 may be due to a physiological stress while metabolizing Fe(II) close to the lower limit of pH for growth, 6.0 (Muehe et al., 2009). The other pH values studied are within or close to the pH range for optimal growth (7.0–7.5) and distant from the upper limit (pH 9.0) (Muehe et al., 2009), and no extensive lag period in Fe(II) oxidation was observed.

Although the solution pH was tested within a fairly narrow range (6.3–7.7), pH had a profound effect on Fe(III) mineral identity (Fig. 5). Consistent with the previous experiment in Fig. 2, lepidocrocite and a small amount of goethite were formed at pH 7.0. However, a slightly acidic condition resulted in entirely lepidocrocite without any goethite. This lack of goethite at pH 6.3 is consistent with the pH requirements for lepidocrocite precipitation: pure lepidocrocite is usually synthesized by aerial oxidation of Fe(II) at pH values no greater than 6.9, above which other iron phases may form (Schwertmann and Cornell, 2000). In addition, the lack of goethite may be due to a diminished influence of dissolved carbonate species (from acetate oxidation) or possibly carboxyl functional groups on the cell membrane. At pH 6.3, slightly below the H_2CO_3–HCO_3^- pK_a of 6.4, the dissolved carbonate species would be shifted away from mostly bicarbonate at pH 7.0 to a higher fraction of carbonic acid, which, as a neutral molecule, has less affinity for Fe(III) (hydr)oxide surfaces.

In contrast, BoFeN1 cells at pH 7.7 produced goethite in a greater abundance than lepidocrocite. This higher solution pH not only affected the mineralogy of the final Fe(III) (hydr)oxide but also resulted in the formation of an intermediate iron phase, blue–green in color that formed within the first 3 h of Fe(II) oxidation and turned into a yellow–orange color shortly thereafter. Although no solid sample was taken to confirm its identity, the color is reminiscent of green rust, a layered, mixed-valent iron hydroxide that can form within anaerobic solutions of Fe(III), aqueous Fe(II), and anions for interlayer charge neutralization (Génin et al., 1998). Green rust previously has been

Table 2
Model parameters for Mössbauer spectra of Fe(III) minerals formed from oxidation of aqueous Fe(II) by *Acidovorax* sp. BoFeN1 within cell suspensions listed in Table 1.

Sample No.	Additive (mM)	Γ[a] (mm s^{-1})	Lepidocrocite						Goethite					
			$\langle CS \rangle$[b] (mm s^{-1})	$\langle QS \rangle$[c] (mm s^{-1})	$\langle H \rangle$[d] (T)	No. of comp.[e]	H_p[f] (T)	Abundance (%)	$\langle CS \rangle$ (mm s^{-1})	$\langle QS \rangle$ (mm s^{-1})	$\langle H \rangle$ (T)	No. of comp.	H_p (T)	Abundance (%)
Vary reaction time														
1[g]	—	0.10	—	—	—	—	—	—	—	—	—	—	—	—
2	—	0.22	0.50	0.02	43.8	3	45.3	69	0.51	−0.20	49.3	2	49.5	28
3	—	0.20	0.50	0.02	43.5	3	44.9	80	0.51	−0.20	49.8	2	49.9	20
4	—	0.20	0.50	0.02	42.9	3	44.6	86	0.51	−0.20	49.5	2	49.8	14
5	—	0.19	0.50	0.02	43.2	3	44.5	90	0.50	−0.20	49.5	2	49.7	10
Vary solution pH														
6	—	0.19	0.50	0.02	43.1	4	45.4	100	—	—	—	—	—	—
7	—	0.21	0.50	0.02	43.1	4	45.3	93	0.50	−0.22	49.9	2	49.9	7
8	—	0.23	0.50	0.02	43.7	3	45.3	42	0.50	−0.22	50.0	2	50.4	58
Vary total CO_3 concentration														
9	—	0.22	0.50	0.02	43.5	3	45.4	94	0.50	−0.22	49.7	2	50.0	6
10	0.2	0.21	0.50	0.02	43.3	3	45.2	92	0.50	−0.22	50.0	2	50.2	8
11	1.0	0.19	0.50	0.02	43.3	3	45.3	90	0.50	−0.22	50.2	1	50.2	10
12	3.0	0.17	0.50	0.02	43.3	3	45.1	83	0.50	−0.22	50.4	1	50.4	17
Vary total PO_4 concentration														
13	—	0.14	0.50	0.01	42.7	4	49.4	91	0.50	−0.22	50.1	1	50.1	9
14	0.2	—	—	—	—	—	—	—	—	—	—	—	—	—
15	1.0	—	—	—	—	—	—	—	—	—	—	—	—	—
16[h]	3.0	—	—	—	—	—	—	—	—	—	—	—	—	—
Vary PPHA concentration														
17	—	0.21	0.50	0.02	43.1	4	45.3	93	0.50	−0.22	49.9	2	49.9	7
18	0.2	0.22	0.50	0.02	43.0	4	45.3	87	0.50	−0.22	49.9	2	50.1	13
19	1.0	0.21	0.50	0.01	43.3	4	44.9	45	0.50	−0.22	49.9	2	50.0	55
20	3.0	—	—	—	—	—	—	—	—	—	—	—	—	—

[a] Lorenztian half-width at half-maximum.
[b] Average center shift.
[c] Average quadrupole splitting. Here, $\langle QS \rangle = 2 \times$ (quadrupole shift).
[d] Average hyperfine magnetic field.
[e] Number of Voigt-based components used to model the hyperfine magnetic field.
[f] Most probable hyperfine magnetic field value.
[g] At an analysis temperature of 77 K, the spectrum contained an Fe(II) doublet with $\langle CS \rangle = 1.32$ mm s^{-1}, $\langle QS \rangle = 2.92$ mm s^{-1} and an Fe(III) doublet with $\langle CS \rangle = 0.48$ mm s^{-1}, $\langle QS \rangle = 0.76$ mm s^{-1}. Here, $\langle QS \rangle$ refers to the average quadrupole splitting distribution.
[h] At an analysis temperature of 77 K, the spectrum contained two Fe(II) doublets that resembled the paired Fe(II) octahedra ($\langle CS \rangle = 1.34$ mm s^{-1}, $\langle QS \rangle = 3.29$ mm s^{-1}) and the isolated Fe(II) octahedra ($\langle CS \rangle = 1.30$ mm s^{-1}, $\langle QS \rangle = 2.56$ mm s^{-1}) in vivianite. An Fe(III) doublet was also observed with ($\langle CS \rangle = 0.55$ mm s^{-1}, $\langle QS \rangle = 0.55$ mm s^{-1}. Here, $\langle QS \rangle$ refers to the average quadrupole splitting distribution.

observed to form by oxidation of Fe(II) by a nitrate-reducing bacterium (Chaudhuri et al., 2001; Weber et al., 2006). BoFeN1 likely precipitated a small amount of Fe(III) that, in the presence of much higher aqueous Fe(II) concentration, was reductively dissolved and re-precipitated as green rust with possibly chloride (Génin et al., 1998) as the interlayer anion. Green rusts can reduce nitrate (Hansen et al., 1996) and nitrite (Hansen et al., 1994) and be oxidized to goethite (Hansen et al., 1994), reactions that possibly contributed to the greater abundance of goethite at this pH.

3.5. Influence of carbonate species

Dissolved carbonate species up to a concentration of 3.0 mM did not significantly affect the rate of Fe(II) oxidation by BoFeN1 cells (Fig. 4). The Fe(II) oxidation rates were nearly identical for all suspensions containing carbonate species, and their oxidation extents were slightly greater than when carbonate species were not added. The lack of any change in Fe(II) oxidation rate suggests that any change in Fe(II) speciation by carbonate species (such as formation of aqueous $Fe(CO_3)_2^{2-}$, which can be oxidized by O_2 more rapidly than aqueous Fe^{2+} or $FeOH^+$ at pH 7 (King, 1998)), does not significantly affect bacterial oxidation of Fe(II). Note that the actual total carbonate concentrations may somewhat deviate from the initial added ones due to production of bicarbonate from acetate oxidation or due to consumption of carbonate species by BoFeN1 if a small amount of carbon fixation occurred. In addition, some of the added carbonate may have partitioned to the

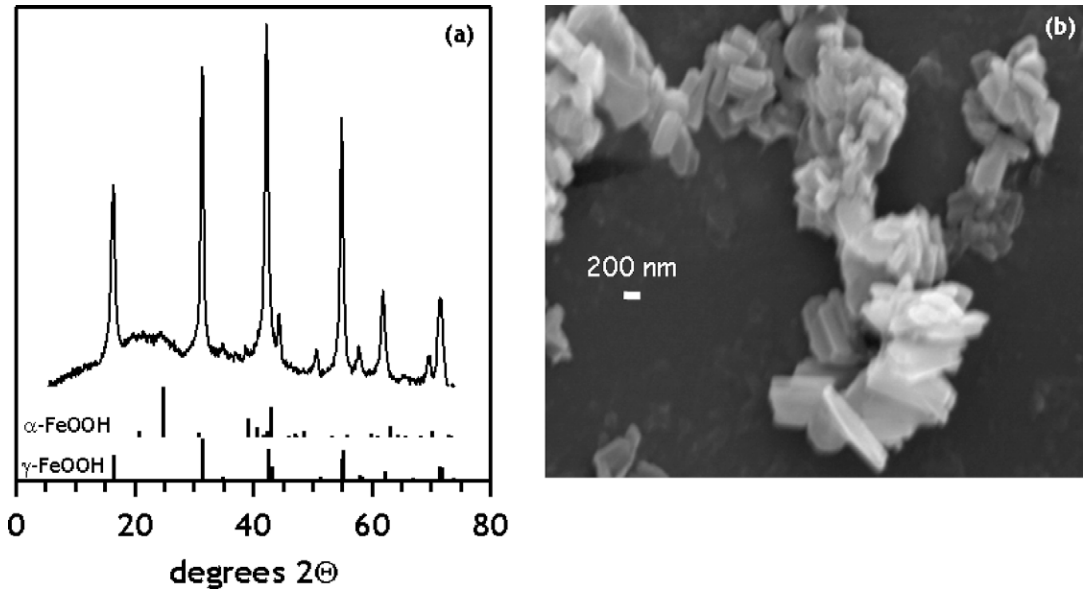

Fig. 3. X-ray diffraction pattern (a) and scanning electron microscope image (b) of solids sampled after 36 h from the batch reactor in Fig. 1.

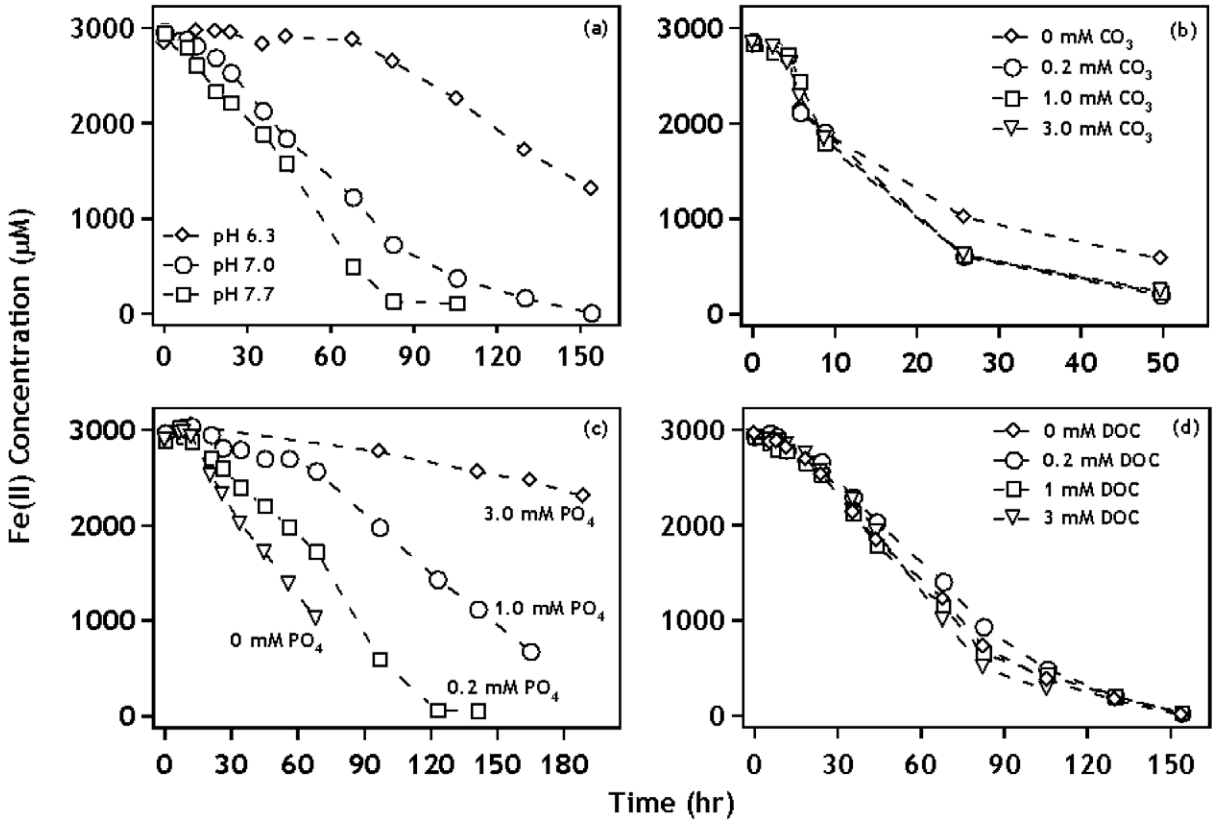

Fig. 4. Fe(II) loss over time for cell suspensions with varying pH (a), carbonate species (b), phosphate species (c), and dissolved organic carbon (added as Pahokee Peat Humic Acid) (d) concentrations. The data plotted for the 3.0 mM PO_4 cell suspension is total (dissolved and solid) Fe(II); all other data points are aqueous Fe(II). Additional information for solution conditions is given in Table 1.

headspace as CO_2. Interestingly, no visible white precipitate formed after addition of carbonate species to the prepared Fe(II) solution despite the solutions being about 10–200 times oversaturated with respect to siderite ($FeCO_{3(s)}$). Lepidocrocite was the dominant Fe(III) phase formed after 50 h, regardless of whether carbonate was added or not

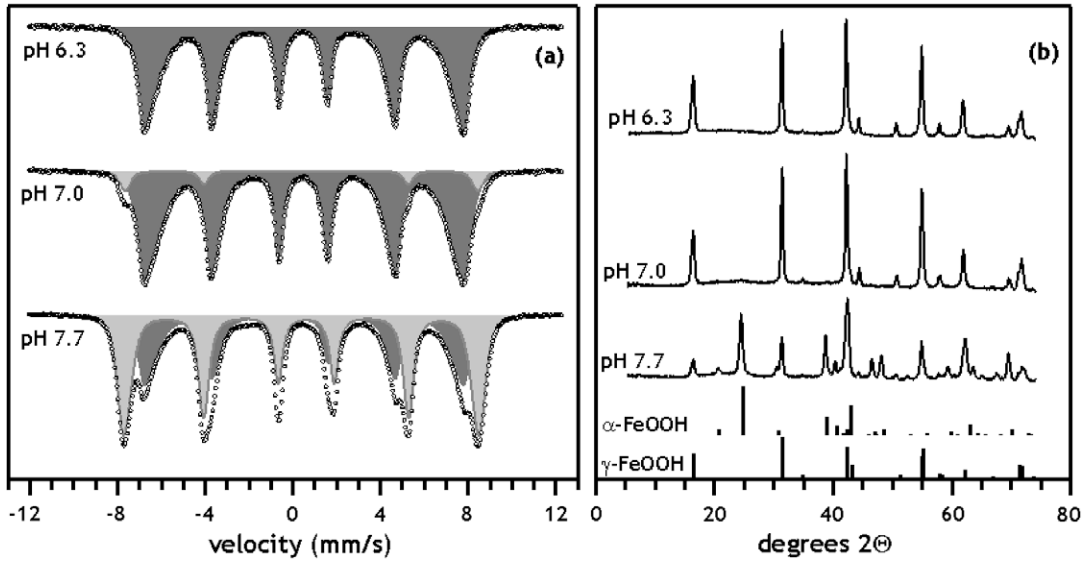

Fig. 5. Mössbauer spectra (a) and X-ray diffraction patterns (b) of minerals formed with varying solution pH. In Mössbauer spectra, dark grey sextets are lepidocrocite and light grey sextets are goethite. Analysis temperature was 4.5 K. Additional information for solution conditions is in Table 1 and Mössbauer parameters are reported in Table 2.

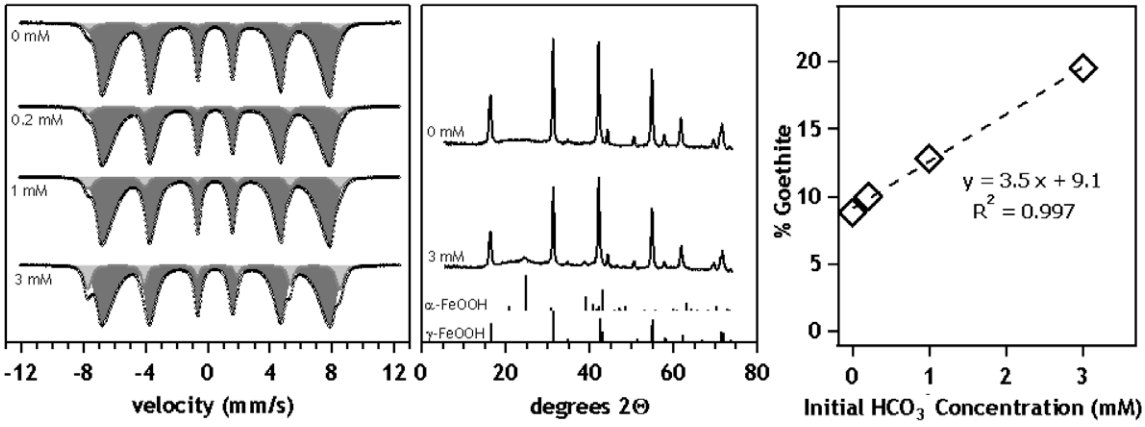

Fig. 6. Mössbauer spectra (a), X-ray diffraction patterns (b), and abundance of goethite (c) within the minerals formed with varying total carbonate concentrations. In Mössbauer spectra, dark grey sextets are lepidocrocite and light grey sextets are goethite. Analysis temperature was 4.5 K. Additional information for solution conditions is in Table 1 and Mössbauer parameters are reported in Table 2.

(Fig. 6a and b). However, the relative abundances of lepidocrocite and goethite changed with respect to carbonate content (Fig. 6c). The proportion of goethite increased linearly with increasing total concentration of carbonate species, indicating that a form of carbonate, likely bicarbonate at this pH, promoted the formation of goethite at the expense of lepidocrocite during the nucleation and growth of Fe(III) crystallites. This relationship between dissolved carbonate content and goethite abundance was previously observed for the aerial oxidation of aqueous Fe(II) (Carlson and Schwertmann, 1990), and equimolar concentrations of bicarbonate and Fe(II) at pH 7.0 were sufficient to completely inhibit lepidocrocite and form only goethite. Here, at most only 20% of the formed Fe(III) was present as goethite when aqueous Fe(II) was equal to the added total carbonate concentration (82% of which was bicarbonate at pH 7.0) possibly because the actual aqueous phase concentration of carbonate species had decreased due to loss by metabolism or volatilization. In other cell suspension studies where pure goethite formed after bacterial oxidation of Fe(II), added bicarbonate concentrations were much higher, around 40 mM with a 80/20 N_2/CO_2 headspace (Senko et al., 2005a,b). Lastly, it is unknown whether our use of a Mops buffer influenced goethite formation compared to the use of an automatic NaOH titrator in Carlson and Schwertmann (1990).

3.6. Influence of phosphate species

The rate of Fe(II) oxidation was progressively slower with increasing amount of phosphate added (Fig. 4). The slower kinetics is likely due to the sequestration of aqueous

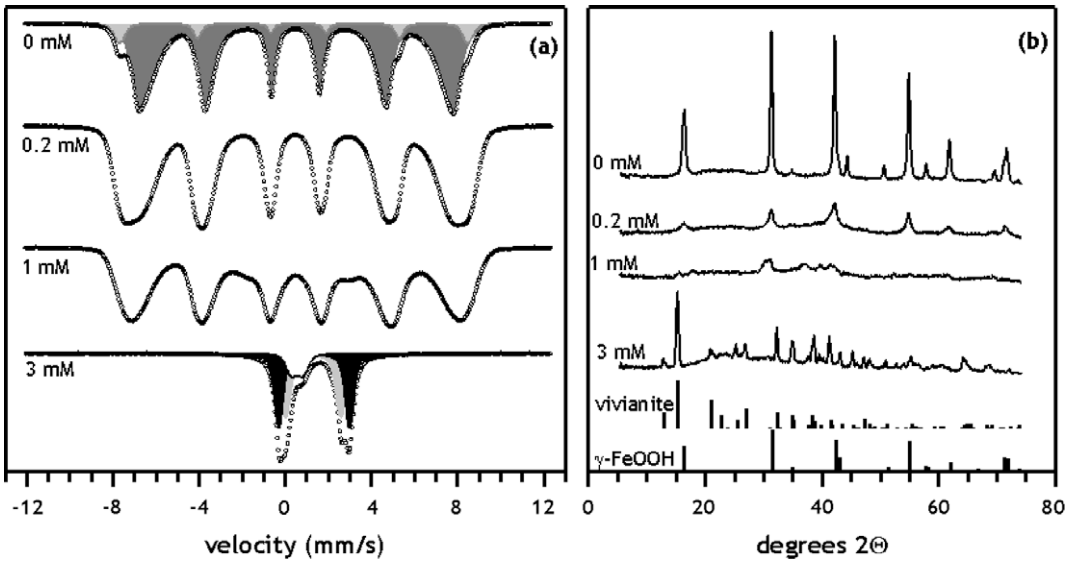

Fig. 7. Mössbauer spectra (a) and μ-X-ray diffraction patterns (b) of minerals formed with varying total phosphate concentrations. In the Mössbauer spectrum for 0 mM total phosphate, the dark grey sextet is lepidocrocite and the light grey sextet is goethite. For 3.0 mM total phosphate, the black doublet is the paired Fe(II) sites in vivianite, the light grey doublet is the isolated Fe(II) sites in vivianite, and the white doublet is an unidentified Fe(III) specie. Analysis temperature was 4.5 K for the 0, 0.2, and 1.0 mM total phosphate suspensions and 77 K for the 3.0 mM total phosphate suspension. Additional information for solution conditions is in Table 1 and Mössbauer parameters are reported in Table 2.

Fe(II) into a solid Fe(II)-phosphate phase that may have limited the bioavailability of Fe(II). A white precipitate had formed shortly after addition of phosphate to the Fe(II) solutions, which became 10^{11}–10^{13} times oversaturated with respect to vivianite ($Fe_3(PO_4)_{2(s)}$). Within the reactor containing 3.0 mM total phosphate, the majority of Fe(II) was found to be in the solid phase after 165 h, only 77 μM of aqueous Fe(II) was detected, compared to 2500 μM total Fe(II) (aqueous plus solid). Note that Fig. 4c reports only total Fe(II) concentrations for the 3.0 mM total phosphate reactor and aqueous Fe(II) concentrations for other reactors.

BoFeN1 cells oxidized Fe(II) to Fe(III) when total phosphate concentrations were present as high as 1.0 mM and only partially oxidized Fe(II) at 3.0 mM total phosphate. Mössbauer spectra (Fig. 7) reveal the formation of purely Fe(III)-bearing phases evidenced by the Fe(III) sextet patterns for the solids taken from reactors containing 0, 0.2, and 1.0 mM total phosphate. Any remaining Fe(II) was likely within the aqueous phase because no evidence of Fe(II)-bearing solids, such as vivianite, was found within the solid phase. However, Fe(III) mineral identification beyond noting the oxidation state was not possible whenever phosphate was present. Lepidocrocite and a minor amount of goethite were detected in 0 mM total phosphate, but at higher phosphate concentrations the Fe(III) sextet signals were too broad for an unambiguous identification of any iron (hydr)oxide. μ-XRD patterns (Fig. 7b) do reveal some lepidocrocite, but not goethite, formation for 0.2 and 1.0 mM total phosphate concentrations. However, the reflection peaks are severely diminished and broadened, indicating either a decrease in crystallite size or crystallinity. Any other possible phases, such as Fe(III)-phosphate or ferrihydrite, are too disordered or amorphous for detection with μ-XRD. It is possible that lepidocrocite and goethite formed with a structure disordered by phosphate incorporation that interrupted long-range Fe(III)–Fe(III) magnetic interactions, thereby disturbing their hyperfine magnetic fields and leading to the observed Mössbauer peak broadening. The peak broadening could also result from lepidocrocite or goethite having a collectively broad distribution of hyperfine magnetic fields due to nanometer-sized crystallite dimensions. Most likely, the broad Fe(III) sextets represent a disordered or amorphous Fe(III)-phosphate solid similar to the one observed to form when BoFeN1 oxidized Fe(II) in a high phosphate content and characterized by scanning transmission X-ray microscopy (Miot et al., 2009a). Phosphate species are expected to affect Fe(III) mineralogy here because they previously have been observed to alter Fe(III) crystallinity during Fe(II) oxidation (Châtellier et al., 2004) and Fe(III) precipitation (Thibault et al., 2009) and have been speculated to influence nitrate-reducing, Fe(II)-oxidizing bacteria (Senko et al., 2005a). Solid-phase phosphate accumulation was confirmed at the end of the experiment by observing complete removal of phosphate from the aqueous phase in the 0.2 and 1.0 mM total phosphate suspensions.

At the highest phosphate concentration, an abundant white precipitate formed initially, and little Fe(II) oxidation was observed. After 8 days, BoFeN1 cells oxidized only 20% of initial Fe(II), and vivianite was the primary solid iron solid. The low extent of Fe(II) oxidation suggests that resting BoFeN1 cells had difficulty accessing Fe(II) within vivianite. Vivianite was readily identified by μ-XRD reflections and within Mössbauer spectra, which showed a pair of Fe(II) doublet peaks nearly identical to synthetic

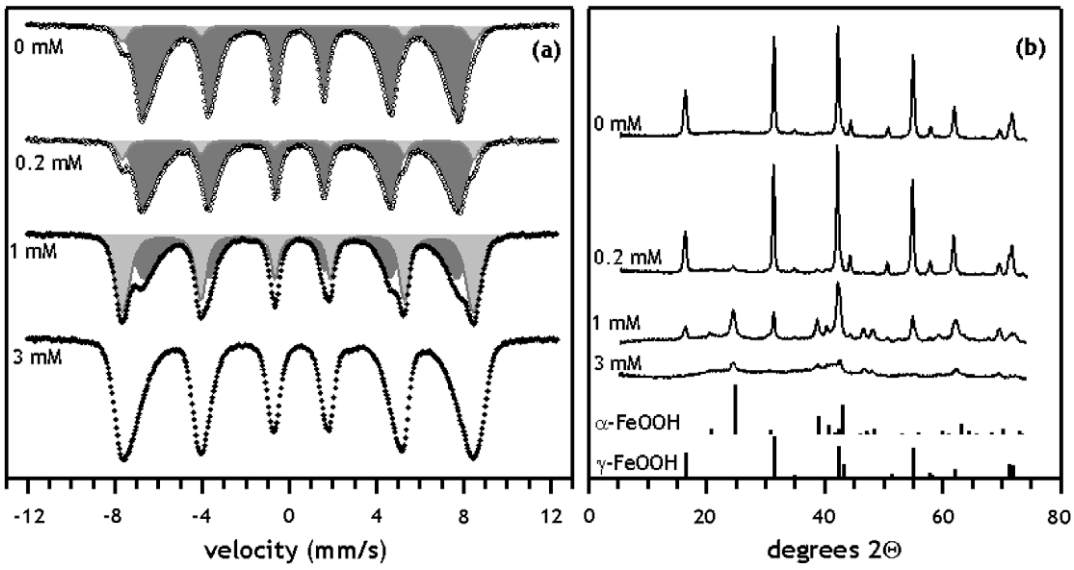

Fig. 8. Mössbauer spectra (a) and μ-X-ray diffraction patterns (b) of minerals formed with varying humic acid concentrations. The concentration values in both parts refer to dissolved organic carbon concentration. In Mössbauer spectra, the dark grey sextets are lepidocrocite and the light grey sextets are goethite. Analysis temperature was 4.5 K. Additional information for solution conditions is in Table 1 and Mössbauer parameters are reported in Table 2.

vivianite (Mattievich and Danon, 1977). Note that this spectrum was collected at 77 K, as opposed to 4.5 K for the others in Fig. 7, in order to present the more clearly identifiable Fe(II) doublets of vivianite as opposed to its rather unformulated octet features at 4.5 K (data not shown). Fe(III) formation was evidenced by a Fe(III) doublet, but its identification was not ascertained because its modeled Mössbauer parameters resembled many Fe(III) (hydr)oxides and possibly Fe(III)-phosphate (Table 2).

3.7. Influence of humic acid

Similar to carbonate species, addition of PPHA did not significantly influence Fe(II) oxidation rates (Fig. 4d). Humic acids generally complex aqueous Fe(II) weakly, and with our low amounts of dissolved PPHA, it is likely that the complexation between dissolved Fe(II) and dissolved humic acids was scarce or too weak to enhance Fe(II) speciation or bioavailability to a significant extent. Dissolved natural organic matter can enhance the rate of Fe(II) oxidation by O_2 but at far lower Fe(II) concentrations (μM to nM) and thus higher DOC:Fe(II) ratios (Rose and Waite, 2003; Craig et al., 2009) than those here.

Addition of 0.2 mM DOC did not significantly alter Fe(III) mineralogy (Fig. 8), as lepidocrocite and goethite were formed in similar proportions as when no PPHA was added. A change in Fe(III) mineral identity and crystallinity was observed at higher concentrations of PPHA. A concentration of 1.0 mM DOC directed the mineral formation from primarily lepidocrocite to mostly goethite, indicated in both the Mössbauer spectrum and μ-XRD pattern. Because humic acids have a strong affinity for mineral surfaces, sorption of the humics likely interfered with the nucleation and crystal growth of Fe(III) and thereby directed the formation of goethite. The incorporation of organic carbon molecules can significantly disrupt the crystallinity and hyperfine magnetic order of Fe(III) precipitates (Schwertmann et al., 2005; Mikutta et al., 2008), and a concentration of 3.0 mM DOC was high enough to prevent complete mineral identification with Mössbauer and μ-XRD. Some broad, minute reflections of goethite are apparent within the μ-XRD pattern, and the corresponding Mössbauer Fe(III) sextet signal has broadened, poorly defined peaks, indicating a disturbed hyperfine magnetic field. Loss of DOC was not measured due to the high concentration of Mops buffer and the formation of bacterial exudates that would confound measurements, but DOC incorporation into the Fe(III) precipitates likely occurred based on the visual observation of the suspensions becoming less dark over time.

4. CONCLUDING REMARKS

Acidovorax sp. BoFeN1 oxidizes aqueous Fe(II) that precipitates primarily as the crystalline Fe(III) (hydr)oxide lepidocrocite. Lepidocrocite formation by microbial Fe(II) oxidation is consistent with lepidocrocite formation by abiotic Fe(II) oxidation with O_2, and we conclude that the bulk geochemical solution condition is responsible for the mineralogy of most of the Fe(III) precipitates. Bacteria metabolic reactions, bacterial exudates, or cell membrane surfaces exerted less influence on the identity or crystallinity of the Fe(II) oxidation products. Some of these biological factors may be responsible for the small quantities of goethite formation or may have restricted the Fe(III) crystallite size, which was shown to lessen for lepidocrocite (Châtellier et al., 2001) and ferrihydrite (Rancourt et al., 2005) formed by Fe(II) oxidation by O_2 in the presence of *Bacillus subtilis* cells.

The relative importance of biotic and abiotic factors controlling Fe(III) precipitation likely differs among the

intracellular, near-surface, and bulk solution regions of Fe(III) precipitation. Fe(III) precipitation associated with or on cell surfaces are certainly influenced by cellular material such as specific functional groups (Chan et al., 2004), but Fe(III) precipitation away from cellular material remains governed by bulk geochemical solution conditions. To better understand these different Fe(III) precipitation processes, mineral spatial identification and greater image resolution is needed between the iron (hydr)oxides and the cell surfaces (Miot et al., 2009b; Schaedler et al., 2009). The lepidocrocite and goethite within our cell suspensions may have precipitated in different locations and therefore likely have different spatial distributions, which may be observable with scanning transmission X-ray microscopy or high-resolution transmission electron microscopy. Directly identifying Fe(III) minerals at specific locations after bacterial Fe(II) oxidation may help us understand the evolution of different Fe(III) phases over time, the onset of cell encrustation by Fe(III) (Schaedler et al., 2009), and any exopolymer templating ability (Chan et al., 2004, 2009).

The geochemical conditions of the medium used in growth experiments and cell suspension experiments should be closely considered when evaluating the Fe(III) mineral identity and crystallinity. For example, goethite formation may be best explained by total carbonate concentration (Carlson and Schwertmann, 1990), and all published studies reporting goethite formation by Fe(II)-oxidizing bacteria contained bicarbonate as a buffer (Kappler and Newman, 2004; Kappler et al., 2005; Senko et al., 2005a,b; Hohmann et al., 2010). Our results confirm goethite is favored at higher total carbonate concentrations during bacterial Fe(II) oxidation. Our results also show that dissolved phosphate, even at sub-millimolar concentrations, can produce poorly crystalline Fe(III) solids during bacterial Fe(II) oxidation (consistent with abiotic Fe(II) oxidation and Fe(III) precipitation (Châtellier et al., 2004; Thibault et al., 2009)) and may explain the lack of Fe(III) crystallinity observed in other cultures containing phosphate (Croal et al., 2004; Miot et al., 2009a,b; Posth et al., 2010).

In general, anions and organic substances coprecipitating with Fe(III) (hydr)oxides may disrupt mineral identity and crystallinity by sorption during initial Fe(III) (hydr)oxide nucleation and preventing full crystal development (for a review, see Cornell and Schwertmann, 2003). We speculate that these coprecipitation processes occurred during Fe(III) precipitation outside of the cell membrane and best explain the Fe(III) mineralogy in the presence of carbonate, phosphate, and humic substances. Dissolved constituents not tested here that also may alter Fe(III) mineralogy are dissolved silica (Schwertmann and Thalmann, 1976; Châtellier et al., 2004), sulfate, and chloride (Xiong et al., 2008). Others proposed that different oxidation rates might explain different mineral identity and crystallinity (Lack et al., 2002; Senko et al., 2005a). Senko et al. (2005a) did show convincingly with a different nitrate-reducing, Fe(II)-oxidizing organism that the cell number density, and concomitantly the Fe(II) oxidation rate, may control Fe(III) crystallinity as measured with X-ray diffraction. Here, crystalline lepidocrocite and goethite were formed in a number of similar cell density and solution conditions with near-complete oxidation of 3 mM Fe(II) occurring within 36–100 h, suggesting this range of oxidation rates is not important to Fe(III) mineralogy formed by BoFeN1 cells.

Finally, the mineralogy of natural Fe(III) (hydr)oxides may be partly driven by the prevailing geochemical solution conditions where Fe(II)-oxidizing bacteria are active. Natural iron (hydr)oxides generally are poorly crystalline, nanosized, often associated with cellular material, and mixtures of phases such as ferrihydrite with goethite or akaganeite (Emerson and Revsbech, 1994; Banfield et al., 2000; Kennedy et al., 2003; Chan et al., 2004; Hallberg and Ferris, 2004). Goethite can transform from ferrihydrite over time (Banfield et al., 2000), but another explanation for natural goethite formation is by direct microbial oxidation of Fe(II) under elevated solution pH or elevated amounts of dissolved carbonate species or humic acids. The coprecipitation of dissolved oxyanions and humic acids also offer an explanation for the poor (or disordered) crystallinity (as indicated by a lack of XRD reflections) of natural iron (hydr)oxides.

ACKNOWLEDGMENTS

The authors thank Katja Amstätter, Inga Kohler, Christoph Berthold for μ-X-ray diffraction measurements, Nikolas Hagemann and Hartmut Schulz for scanning electron microscopy measurements, Florian Hegler for BoFeN1 cell cultivation assistance, Dijie Liao for phosphate measurements, and the three anonymous reviewers whose suggestions improved the manuscript. Funding was provided by the Deutsche Forschungsgemeinschaft by Grant HA 3453/5-1.

APPENDIX A. SUPPLEMENTARY DATA

Supplementary data associated with this article can be found, in the online version, at doi:10.1016/j.gca.2010.03.037.

REFERENCES

Banfield J. F., Welch S. A., Zhang H., Ebert T. T. and Penn R. L. (2000) Aggregation-based crystal growth and microstructure development in natural iron oxyhydroxide biomineralization products. *Science* **289**, 751–754.

Carlson L. and Schwertmann U. (1990) The effect of CO_2 and oxidation rate on the formation of goethite versus lepidocrocite from an Fe(II) system at pH 6 and 7. *Clay Miner.* **25**, 65–71.

Chan C. S., De Stasio G., Welch S. A., Girasole M., Frazer B. H., Nesterova M. V., Fakra S. and Banfield J. F. (2004) Microbial polysaccharides template assembly of nanocrystal fibers. *Science* **303**, 1656–1658.

Chan C. S., Fakra S. C., Edwards D. C., Emerson D. and Banfield J. F. (2009) Iron oxyhydroxide mineralization on microbial extracellular polysaccharides. *Geochim. Cosmochim. Acta* **73**, 3807–3818.

Charlet L. and Manceau A. (1992) X-ray absorption spectroscopic study of the sorption of Cr(III) at the oxide–water interface: II. Adsorption, coprecipitation, and surface precipitation on hydrous ferric oxide. *J. Colloid Interface Sci.* **148**, 443–458.

Châtellier X., Fortin D., West M. M., Leppard G. G. and Ferris F. G. (2001) Effect of the presence of bacterial surfaces during the synthesis of Fe oxides by oxidation of ferrous ions. *Eur. J. Mineral.* **13**, 705–714.

Châtellier X., West M. M., Rose J., Fortin D., Leppard G. G. and Ferris F. G. (2004) Characterization of iron-oxides formed by oxidation of ferrous ions in the presence of various bacterial species and inorganic ligands. *Geomicrobiol. J.* **21**, 99–112.

Chaudhuri S. K., Lack J. G. and Coates J. D. (2001) Biogenic magnetite formation through anaerobic biooxidation of Fe(II). *Appl. Environ. Microb.* **67**, 2844–2848.

Coby A. J. and Picardal F. W. (2005) Inhibition of NO_3^- and NO_2^- reduction by microbial Fe(III) reduction: evidence of a reaction between NO_2^- and cell surface-bound Fe^{2+}. *Appl. Environ. Microb.* **71**, 5267–5274.

Cornell R. M. and Schwertmann U. (2003) *The Iron Oxides: Structure, Properties, Reactions, Occurrences and Uses*. Wiley-VCH Verlag GmbH, Weinheim.

Craig P. S., Shaw T. J., Miller P. L., Pellechia P. J. and Ferry J. L. (2009) Use of multiparametric techniques to quantify the effects of naturally occurring ligands on the kinetics of Fe(II) oxidation. *Environ. Sci. Technol.* **43**, 337–342.

Croal L. R., Johnson C. M., Beard B. L. and Newman D. K. (2004) Iron isotope fractionation by Fe(II)-oxidizing photoautotrophic bacteria. *Geochim. Cosmochim. Acta* **68**, 1227–1242.

Ehrenreich A. and Widdel F. (1994) Anaerobic oxidation of ferrous iron by purple bacteria, a new type of phototrophic metabolism. *Appl. Environ. Microb.* **60**, 4517–4526.

Emerson D. and Moyer C. L. (2002) Neutrophilic Fe-oxidizing bacteria are abundant at the Loihi seamount hydrothermal vents and play a major role in Fe oxide deposition. *Appl. Environ. Microb.* **68**, 3085–3093.

Emerson D. and Revsbech N. P. (1994) Investigation of an iron-oxidizing microbial mat community located near Aarhus, Denmark: field studies. *Appl. Environ. Microb.* **60**, 4022–4031.

Emerson D. and Weiss J. V. (2004) Bacterial iron oxidation in circumneutral freshwater habitats: findings from the field and the laboratory. *Geomicrobiol. J.* **21**, 405–414.

Génin J.-M. R., Bourrié G., Trolard F., Abdelmoula M., Jaffrezic A., Refait P., Maitre V., Humbert B. and Herbillon A. (1998) Thermodynamic equilibria in aqueous suspensions of synthetic and natural Fe(II)–Fe(III) green rusts: occurrences of the mineral in hydromorphic soils. *Environ. Sci. Technol.* **32**, 1058–1068.

Good N. E. and Izawa S. (1972) Hydrogen ion buffers. *Methods Enzymol.* **24**, 53–68.

Hallberg R. and Ferris F. G. (2004) Biomineralization by *Gallionella*. *Geomicrobiol. J.* **21**, 325–330.

Hansen H. C. B., Borggaard O. K. and Sørensen J. (1994) Evaluation of the free energy of formation of Fe(II)–Fe(III) hydroxide-sulfate (green rust) and its reduction of nitrite. *Geochim. Cosmochim. Acta* **58**, 2599–2608.

Hansen H. C. B., Koch C. B., Nancke-Kroge H., Borggaard O. K. and Sørensen J. (1996) Abiotic nitrate reduction to ammonium: key role of green rust. *Environ. Sci. Technol.* **30**, 2053–2056.

Hegler F., Posth N., Jiang J. and Kappler A. (2008) Physiology of phototrophic iron(II)-oxidizing bacteria: implications for modern and ancient environments. *FEMS Microbiol. Ecol.* **66**, 250–260.

Hohmann C., Winkler E., Morin G. and Kappler A. (2010) Anaerobic Fe(II)-oxidizing bacteria show As resistance and co-precipitate As during Fe(III) mineral precipitation. *Environ. Sci. Technol.* **44**, 94–101.

Kappler A. and Newman D. K. (2004) Formation of Fe(III)-minerals by Fe(II)-oxidizing photoautotrophic bacteria. *Geochim. Cosmochim. Acta* **68**, 1217–1226.

Kappler A., Schink B. and Newman D. K. (2005) Fe(III) mineral formation and cell encrustation by the nitrate-dependent Fe(II)-oxidizer strain BoFeN1. *Geobiology* **3**, 235–245.

Kappler A., Johnson C. M., Crosby H. A., Beard B. L. and Newman D. K. (2010) Evidence for equilibrium iron isotope fractionation by nitrate-reducing iron(II)-oxidizing bacteria. *Geochim. Cosmochim. Acta.* **74**, 2826–2842.

Kennedy C. B., Martinez R. E., Scott S. D. and Ferris F. G. (2003) Surface chemistry and reactivity of bacteriogenic iron oxides from Axial volcano, Juan de Fuca ridge, north-east Pacific Ocean. *Geobiology* **1**, 59–69.

King D. W. (1998) Role of carbonate speciation on the oxidation rate of Fe(II) in aquatic systems. *Environ. Sci. Technol.* **32**, 2997–3003.

Klausen J., Trober S. P., Haderlein S. B. and Schwarzenbach R. P. (1995) Reduction of substituted nitrobenzenes by Fe(II) in aqueous mineral suspensions. *Environ. Sci. Technol.* **29**, 2396–2404.

Lack J. G., Chaudhuri S. K., Chakraborty R., Achenbach L. A. and Coates J. D. (2002) Anaerobic biooxidation of Fe(II) by *Dechlorosoma suillum*. *Microb. Ecol.* **43**, 424–431.

Laskov C., Herzog C., Lewandowski J. and Hupfer M. (2007) Miniaturized photometrical methods for the rapid analysis of phosphate, ammonium, ferrous iron, and sulfate in pore water of freshwater sediments. *Limnol. Oceanogr. Meth.* **4**, 63–71.

Lovley D. R. (1991) Dissimilatory Fe(III) and Mn(IV) reduction. *Microbiol. Rev.* **55**, 259–287.

Mattievich E. and Danon J. (1977) Hydrothermal synthesis and Moessbauer studies of ferrous phosphates of the homologous series $Fe_3^{2+}(PO_4)_2(H_2O)_n$. *J. Inorg. Nucl. Chem.* **39**, 569–580.

Mikutta C., Mikutta R., Bonneville S., Wagner F., Voegelin A., Christl I. and Kretzschmar R. (2008) Synthetic coprecipitates of exopolysaccharides and ferrihydrite: Part I. Characterization. *Geochim. Cosmochim. Acta* **72**, 1111–1127.

Miot J., Benzerara K., Morin G., Bernard S., Beyssac O., Larquet E., Ona-Nguema G., Kappler A. and Guyot F. (2009a) Transformation of vivianite by anaerobic nitrate-reducing iron-oxidizing bacteria. *Geobiology* **7**, 373–384.

Miot J., Benzerara K., Morin G., Kappler A., Bernard S., Obst M., Ferard C., Skouri-Panet F., Guigner J.-M., Posth N., Galvez M., Brown, Jr., G. E. and Guyot F. (2009b) Iron biomineralization by anaerobic neutrophilic iron-oxidizing bacteria. *Geochim. Cosmochim. Acta* **73**, 696–711.

Miot J., Benzerara K., Obst M., Kappler A., Hegler F., Schaedler S., Bouchez C., Guyot F. and Morin G. (2009c) Extracellular iron biomineralization by photoautotrophic iron-oxidizing bacteria. *Appl. Environ. Microb.* **75**, 5586–5591.

Muehe E. M., Gerhardt S., Schink B. and Kappler A. (2009) Ecophysiology and energetic benefit of mixotrophic Fe(II)-oxidation by nitrate-reducing bacteria. *FEMS Microbiol. Ecol.* **70**, 335–343.

Posth N., Huelin S., Konhauser K. O. and Kappler A. (2010) Size, density and composition of cell–mineral aggregates formed during anoxygenic phototrophic Fe(II) oxidation: impact on modern and ancient environments. *Geochim. Cosmochim. Acta.* **74**, 3476–3493.

Rancourt D. G., Thibault P.-J., Mavrocordatos D. and Lamarche G. (2005) Hydrous ferric oxide precipitation in the presence of nonmetabolizing bacteria: constraints on the mechanism of a biotic effect. *Geochim. Cosmochim. Acta* **69**, 553–577.

Rose A. L. and Waite T. D. (2003) Effect of dissolved natural organic matter on the kinetics of ferrous iron oxygenation in seawater. *Environ. Sci. Technol.* **37**, 4877–4886.

Schaedler S., Burkhardt C., Hegler F., Straub K. L., Miot J., Benzerara K. and Kappler A. (2009) Formation of cell–iron–

mineral aggregates by phototrophic and nitrate-reducing anaerobic Fe(II)-oxidizing bacteria. *Geomicrobiol. J.* **26**, 93–103.

Schwertmann U. and Cornell R. M. (2000) *Iron Oxides in the Laboratory: Preparation and Characterization*. Wiley-VCH Verlag GmbH, Weinheim.

Schwertmann U. and Thalmann H. (1976) The influence of [Fe(II)], [Si], and pH on the formation of lepidocrocite and ferrihydrite during oxidation of aqueous $FeCl_2$ solutions. *Clay Miner.* **11**, 189–200.

Schwertmann U., Wagner F. and Knicker H. (2005) Ferrihydrite–humic associations: magnetic hyperfine interactions. *Soil Sci. Soc. Am. J.* **69**, 1009–1015.

Senko J. M., Dewers T. A. and Krumholz L. R. (2005a) Effect of oxidation rate and Fe(II) state on microbial nitrate-dependent Fe(III) mineral formation. *Appl. Environ. Microb.* **71**, 7172–7177.

Senko J. M., Mohamed Y., Dewers T. A. and Krumholz L. R. (2005b) Role for Fe(III) minerals in nitrate-dependent microbial U(IV) oxidation. *Environ. Sci. Technol.* **39**, 2529–2536.

Sørensen J. and Thorling L. (1991) Stimulation by lepidocrocite (g-FeOOH) of Fe(II)-dependent nitrite reduction. *Geochim. Cosmochim. Acta* **55**, 1289–1294.

Stookey L. L. (1970) Ferrozine—a new spectrophotometric reagent for iron. *Anal. Chem.* **42**, 779–781.

Straub K. L. and Buchholz-Cleven B. E. E. (1998) Enumeration and detection of anaerobic ferrous iron-oxidizing, nitrate-reducing bacteria from diverse European sediments. *Appl. Environ. Microb.* **64**, 4846–4856.

Straub K. L., Schoenhuber W. A., Buchholz-Cleven B. E. E. and Schink B. (2004) Diversity of ferrous iron-oxidizing, nitrate-reducing bacteria and their involvement in oxygen-independent iron cycling. *Geomicrobiol. J.* **21**, 371–378.

Thibault P.-J., Rancourt D. G., Evans R. J. and Dutrizac J. E. (2009) Mineralogical confirmation of a near-P:Fe = 1:2 limiting stoichiometric ratio in colloidal P-bearing ferrihydrite-like hydrous ferric oxide. *Geochim. Cosmochim. Acta* **73**, 364–376.

Weber K. A., Achenbach L. A. and Coates J. D. (2006) Microorganisms pumping iron: anaerobic microbial iron oxidation and reduction. *Nat. Rev. Microbiol.* **4**, 752–764.

Xiong H., Liao Y. and Zhou L. (2008) Influence of chloride and sulfate on formation of akaganeite and schwertmannite through ferrous biooxidation by acidithiobacillus ferrooxidans cells. *Environ. Sci. Technol.* **42**, 8681–8686.

Yu Q., Kandegedara A., Xu Y. and Rorabacher D. B. (1997) Avoiding interferences from Good's buffers: a contiguous series of noncomplexing tertiary amine buffers covering the entire range of pH 3–11. *Anal. Biochem.* **253**, 50–56.

Associate editor: Stephan M. Kraemer